Fig. S1. The necroptotic in MS tissue (Suppl. to Figure 1.) (**A**) Western blotting analysis and quantification of fresh frozen *post mortem* brain lysates (solubilized in Triton/SDS buffer) of normal and white matter lesions from control and MS patients, respectively, for RIPK1 and RIPK3 levels. (**B**) Representative western blotting analysis of control samples and white matter lesions in MS samples for RIPK1 levels in both Triton/SDS-soluble (bottom) and Triton/SDS-insoluble (top) fractions; actin was used as a loading control (right panels). (**C**) Enlarged images of **Fig. 1E**: anti-RIPK1 immunostaining of *post mortem* brain sections from a patient with primary progressive MS. Higher magnification images of the boxed regions are depicted below. (**D**) Immunostaining of *post mortem* cortical near lesion sections from a MS patient and sections of normal appearing white matter (NAWM) from a control individual using anti-RIPK1 and R461 antibody, a human oligodendrocyte marker (upper panels) (He et al., 2004).

Fig. S2. Phosphorylation of the necroptotic machinery as a marker for activation. (Suppl. to Figure 1-3) (**A**) 293T cells transfected with expression vectors of GFP, RIPK1 or kinase dead (K45M) RIPK1 (KD-RIPK1) were treated with either vehicle (-) or TNFα for the indicated periods of times in minutes. The cell lysates were analyzed by western blotting using anti-p-S14/15-RIPK1 and RIPK1. (**B**) Wild-type (WT) or RIPK1 deficient (RIPK1[def]) Jurkat cells were treated with either vehicle (-) or TNFα (T) for 15 minutes with or without 7-Cl-O-Nec-1 (7N-1). The cell lysates were analyzed by western blotting using anti-p-S14/15-RIPK1 and RIPK1. (**C**) Western blotting analysis and

quantification of lysates from cultured rat oligodendrocytes treated with increasing concentrations of mTNFα (100 ng/ml for indicated periods of times in minutes) and probed with anti-p-S14/15-RIPK1, RIPK1 and β-actin. (**D**) 293T cells were transfected with an expression vector for RIPK1. The cell lysates were treated with either lambda phosphatase or vehicle for 30 min at 37°C, and analyzed by western blotting using anti-p-S14/15-RIPK1 and RIPK1. (**E**) 293T cells transfected with expression vectors of wild-type RIPK1 or RIPK1 Ser166Ala (S166A) mutant. The cell lysates were analyzed by western blotting using anti-p-Ser166-RIPK1 and RIPK1. (**F**) HT29 cells were treated with either vehicle or mTNFα (100 ng/ml), SM164 (SMAC mimetic that can promote the degradation of cIAP1/2; 300 nM) and zVAD.fmk (20 uM) to promote the activation of necroptosis in the presence or absence of 7N-1 for 6h. The cell lysates were treated with either lambda phosphatase or vehicle for 30 min at 37°C, and then probed with anti-p-S166-RIPK1 and RIPK1, with anti-p-S227-RIPK3 and RIPK3, and with anti-p-T358-MLKL and MLKL . (**G**) phospho-MLKL immunostaining of *post mortem* brain sections from a control individual showed little immunoreactivity in cortical white matter as a control for Fig. 2A. **(H)** Primary rat neurons, astrocytes (Ast), microglia (Mg) oligodendrocytes (Olig), and mixed cultured cells (Mix) were grown *in vitro* for the indicated number of days; for oligodendrocytes we used both a mixed culture preparation grown in BDM (Mixed BDM), as well as a purified oligodendrocyte population grown in OPC promoting medium (OPC). The cell lysates were prepared and subjected to western blotting analysis. The levels of key mediators of necroptosis, MLKL, RIPK1, and RIPK3, were examined. MBP, NeuN, IBA1 and GFAP were used as markers for oligodendrocytes, neurons, microglia and astrocytes, respectively. Actin was a loading

control. (**I**) Data in the bar graph is the average fold loss or enrichment of selected myelin associated proteins identified by proteomic analysis in the urea fractions of MS compared to that of control samples.

Fig. S3. Protection of mature oligodendryctes by inhibiting RIPK1 kinase. (**A**) Mice **(Suppl. to Figure 4,5)** were on cuprizone-containing diet with or without 7N-1 for 4.5 weeks and the sections of corpus callosum were immunostained with CC1 (green), a marker for mature oligodendrocytes and Hoechst dye for nuclei (blue). The numbers of CC1+ cells in the corpus callosum in the indicated experimental groups were quantified by counting z-series reconstructions with depth of 10 μm using sections from the medial corpus callosum (2 slices per animal, 4-5 animals were used per group) (bar graph on the right). Data are represented as the normalized means ± SEM, (*$p<0.05$, **$p<0.01$) (**B**) Representative images of corpus callosum sections immunostained for the microglial marker, IBA1 and the density of cells/100μm^2 in the CC were quantified. Data are means ± SEM, n=5-8 per group. (*$p<0.05$). (**C**) Mice were fed either control or 0.2 % cuprizone containing diet for 3 weeks, at which point animals were separated into two groups with the same starting weight and behavioral performance was measured on the rotarod for a subsequent 2 weeks. The time until mice fell off the rotarod was recorded. Data are means ± SEM, n=7-9 per group. (*$p<0.05$). The increased ability to stay longer on rotarod with 7N-1 treated group is similar to that of wt mice and reflects learning from daily practice. **(D)** Representative images of sections from medial corpus callosum immunostained with anti-RIPK1 and different cell type markers to show the expression of RIPK1 in various cell types of the CNS including astrocytes (GFAP), microglia

(IBA1), and the cells in the oligodendrocyte lineage (NG2, OPC progenitor cells; Olig2, oligodendrocytes; CC1, oligodendrocytes). The number of each cell type that was also positive for RIPK1 was quantified by counting z-series reconstructions with depth of 10 μm using sections from the medial corpus callosum (30-40 cells were counted per slice; 1-2 slices per animal; 3-4 animals were used per group) (bar graph on the right). Data are represented as fractions of the cells that are positive for RIPK1 divided by the total cell numbers counted for each cell type. (**E**) Representative images of sections from medial CC show the increase of RIPK1 reactivity and ThioS staining, in cuprizone treated animals as compared to control treated animals following 5 weeks of cuprizone treatment. (**F**) Representative images of sections from medial corpus callosum in control and cuprizone treated mice show a more punctate staining of A11, an antibody that recognize a peptide backbone epitope that is common to amyloid oligomers. (**G**) Representative images of sections from medial corpus callosum in control and cuprizone treated mice immunostained with anti-RIPK1 and the amyloid oligomer specific antibody A11. **(H)** Wild-type or RIPK3 KO mice were fed either control or 0.2 % cuprizone containing diet for the indicated times; corpus callosum was microdissected, lysed and sequentially separated as Triton (1%) soluble, RIPA (SDS) soluble and urea soluble fractions and analyzed by western blot analysis using antibodies against RIP1 and normalized to β-actin. The quantifications were shown as bar graphs below. Data are represented as the normalized means ± SEM, n= replicates per group (*$p<0.05$).

Fig. S4. The effect of 7N-1 in the EAE model. (Suppl. to Figure 6) (**A**) Representative images of EAE spinal cord sections immunostained with anti-RIPK1, anti-IBA1 and

DAPI (top) and anti-RIPK1, anti-Olig2 and DAPI (bottom). White box insets depict a higher magnification image. The number of each cell type that was also positive for RIPK1 was quantified by counting z-series reconstructions with depth of 10 μm using sections from the medial corpus callosum (30-40 cells were counted per slice; 1-2 slices per animal; 3-4 animals were used per group) (bar graph on the right). Data are represented as fractions of the cells that are positive for RIPK1 divided by the total cell numbers counted for each cell type. **(B)** The weight of vehicle (veh) and 7N-1 treated animals (from day 0) (**A**) and weight after immunization using MOG 35–55 in CFA from three independent experiments. Data represented as the mean ± SE; n = 8-10 animals per group; to assess statistical difference between vehicle and 7N-1 treated animals, student's t-test was at each time point, (*$p<0.05$, **$p<0.01$). (**C**) Spinal cords of vehicle (veh) and 7N-1 treated animals (dosing starting from day 6 after immunization) after 18 days of treatment were lysed and subjected to ELISA for IL6 and IL1β. Data represented as the mean ± SE; n = 5 animals per group (*$p<0.05$). (**D**) Spleens of either control or MOG immunized animals in the presence of vehicle or 7N-1 for 15-17 days were dissected and representative EAE induced spleens are shown. Spleens were weighed and normalized to animal body weight. Data represented as mean ± SE; n's are depicted for each group. (**E**) Serum MOG peptide reactive antibody was measured by peptide adsorbed ELISA. Splenic cell composition was evaluated after immunization in vehicle and 7N-1 treated animals; experiments were performed in triplicate. (**F**) RBC-lysed splenic cells from animals with indicated treatment were immunostained with markers for B-cells (B220), macrophages (CD11b), and T-cells (CD3), and subjected to FACS analysis. (**G**) RBC-lysed splenic cells were cultured on CD3 coated plates and treated with either vehicle or

MOG peptide and cell number was determined following 96 h of incubation, as well as (**H**) IL6 production by ELISA; experiments were performed on 3-4 animals per experimental group. **(I**) HUVECs were treated with recombinant human TNF α in the presence of either vehicle or 7N-1 and the induction of VCAM was examined by western blotting analysis. Quantification of band intensity showed a robust TNF α - induced VCAM increase which was not affected by 7N-1. Data represented as mean ± SE; n = 3. **(J)** Adoptive transfer of MOG primed GFP-splenocytes and lymphocytes (5 x10^6 cells/ animal) into naïve animals. 7N-1 did not alter the amount of GFP-positive cells in the CNS, as assessed by western blotting analysis of spinal cord lysates for GFP reactivity **(K)** nor the levels of GFP+ percoll isolated mononuclear cells in the spinal cord, as assessed by FACs. Data represented as mean ± SE; n = 3-4 animals per group.

Fig. S5. RIPK3 deficiency attenuates EAE-induced neurological deficit. (Suppl. to Figure 6) (**A**) Representative images of spinal cord sections from control and after EAE induction immunostained with anti-RIPK1, anti-RIPK3 and DAPI to show significantly increased RIPK1 immunostaining after induction of EAE within an inflammatory lesion while RIPK3 immunostaining was not markedly increased following induction of EAE. The cells within an inflammatory lesion in the spinal cord white matter or corresponding area in control spinal cord were identified by DAPI positivity; the percentages of RIPK1 (orange), RIPK3 (blue) or RIPK1, RIPK3 double positive cells (pink) are quantified in a bar graph (129 cells from 6 images from 3 animals were used for the control group, and 1283 cells from 10 images from 5 animals were used for the EAE group). **(B)** The levels of RIPK1 and RIPK3 after the induction of EAE as determined by western blotting

analysis. **(C)** Clinical scores of WT and RIPK3-/- after immunization using MOG 35–55 in CFA. The clinical scores of three experiments were evaluated for 18 days. Data represented as mean ± SE; n = 8 animals per group. To assess statistical difference between vehicle and 7N-1 treated animals, student's t-test was at each time point (*$p<0.05$). (**D**) Splenic cell composition was evaluated after immunization in WT and RIPK3-/- animals. RBC-lysed splenic cells were stained with markers for macrophages (CD11b), B-cells (B220), and T-cells (CD3), and subjected to FACS analysis. Data is summarized in the table. Data represented as mean ± SE; n = 4 animals per group.

Fig. S6. Morphological and biochemical features of oligodendrocyte cell death. (Suppl. to Figure 7) (**A**) Representative image of a primary rat oligodendrocyte immunostained with anti-RIPK1, anti-RIPK3, and MBP and DAPI; the merged image is shown on the right. **(B-C)** Primary mixed rat oligodendrocytes were treated with 100ng/mL(TNF100) of recombinant mouse TNF α or staurosporine (STS; 500 nM). The cell viability was determined by the Toxilight (Lonza) 6 or 24 h after treatment (**B**). The cell lysates were used to assess the levels of pro- and active caspase-3 by western blotting analysis (**C**). STS treatment was a control for caspase-3 activation in apoptosis. **(D)** Oligodendrocytes were pre-treated with 100ng/mL (TNF100) of recombinant mouse TNFα for 3 h and then imaged continuously in the presence of propidium iodide (PI) and *Alexa* Fluor *488 annexin V* for 15 hours. Each image was acquired at 5 min intervals. The first 9 hours of images are shown in the montage. A neighboring dead cell is shown as being PI-positive in all images; the yellow arrows indicate the swelling of the cell, which occurred before it became PI-positive.

Fig. S7. Plasma and CNS levels of 7N-1 following administration of the compound. (Suppl. to Methods for 7N-1 delivery) **(A)** Animals were either given 7N-1 in their drinking water for 24 h ad libitum and either sacrificed in the morning or injected with a single IP injection (10 mg/kg) of 7N-1 and sacrificed at either 1 h or 8 h after the IP injection in the presence of 7N-1 water. 7N-1 levels were assessed in both the plasma and brain by HPLC. Molarity was calculated based on a molecular weight of 270 MW for 7-Cl-O-7N-1. (**B**) Plasma 7N-1 concentrations were analyzed by LC-MS/MS at different time points after a single 7N-1 administration (1 mg/kg). (**C**) Plasma concentration versus time data was subjected to non-compartmental analysis using the pharmacokinetic program WinNonLin v. 4.1 to obtain pharmacokinetic parameters for males and females. Each time point represents a mean of 3 plasma level determinations, from 3 separate mice, sacrificed at the appropriate interval post-dosing.

Supplemental Movie, Table legends:

Movie S1. (Suppl. to Figure 7)

Primary cultured oligodendrocytes were pre-treated with 100ng/mL (TNF100) of recombinant mouse TNFα for 3 h and then imaged continuously in the presence of propidium iodide (PI) and *Alexa* Fluor *488 annexin V*, for 15 hours. Each image was acquired at 5 min intervals. A neighboring dead cell is shown as being PI-positive in all images; the yellow arrows indicate the swelling of the cell, which precedes it becoming PI-positive.

Table S1. The cumulative data from all fresh frozen pathological samples of human control and MS patients analyzed as semi-quantitative measurements using western blot analysis describing the expression of MAG, RIP1 and FLIP$_L$ and caspase-8 (p43/41). (Suppl. to Figure 1) RIP1(s): RIP1 in Triton (1%)/SDS soluble extraction. RIP1(u): RIP1 in the urea fraction and RIP3(u) in the urea fraction. RIP1, Casp8, cFLIP$_L$ and myelin were examined by western blotting analysis. The levels of RIP1, caspase-8 C43 fragment, cFLIP$_L$ and myelin were scored as ++++ (very strong), +++ (strong), ++ (moderate), + (weak), – (no) and N/A (not examined). CTL: age matched human control cases. MS: MS patient samples.

Table S2. **Genes that are differentially regulated in chronic active lesions vs. inactive lesions in MS and have also been identified as regulators of necroptosis. (Suppl. to Figure 1)** The table lists genes that were identified in a microarray study that were up regulated in chronic active lesions vs. inactive lesions (Selmaj and Raine, 1988) and were also identified as either protective against necroptosis (blue, negative z-score) or enhancers of necroptosis (red, positive z-score) in L929 cells (Hitomi et al., 2008).

Table S3. Proteomic analysis of urea soluble proteins that are enriched in MS tissue. (Suppl. to Figure 3) List of proteins that were identified by dimethyl isotope labeling mass spectrometry to be enriched in urea soluble fraction using the sarkosyl extraction protocol in MS brain tissue by greater than 1.5 fold as compared to control tissue. The

samples were prepared by pooling samples from 3 control patients and 3 MS patients and performing two runs on the mass spectrometer. Proteins in red were identified in both runs.

Table S4. Increased components in the insoluble proteome of MS that were also found in Lewy body of pathological brain samples from PD patients. (Suppl. to Figure 3) List of proteins hits present in the insoluble fractions of the MS and LB datasets >1.5-fold of their controls were tabulated.

Table S5. Proteomic analysis of urea soluble proteins that are enriched in MS tissue that are implicated in various neurodegenerative diseases. (Suppl. to Figure 3) Gene ontology KEGG pathway cluster analysis identified proteins that are implicated in various aspects of Alzheimer's, Parkinson's and Huntington's diseases.

Table S6. Putative RIPK3 targets in the insoluble proteome of MS. (Suppl. to Figure 3) RIPK3 logo motif was retrieved from Phosphonetworks database (http://phosphonetworks.org/). Phosphorylation motif logo for hits identified in MS samples were predicted using WebLogo (http://weblogo.berkeley.edu/).

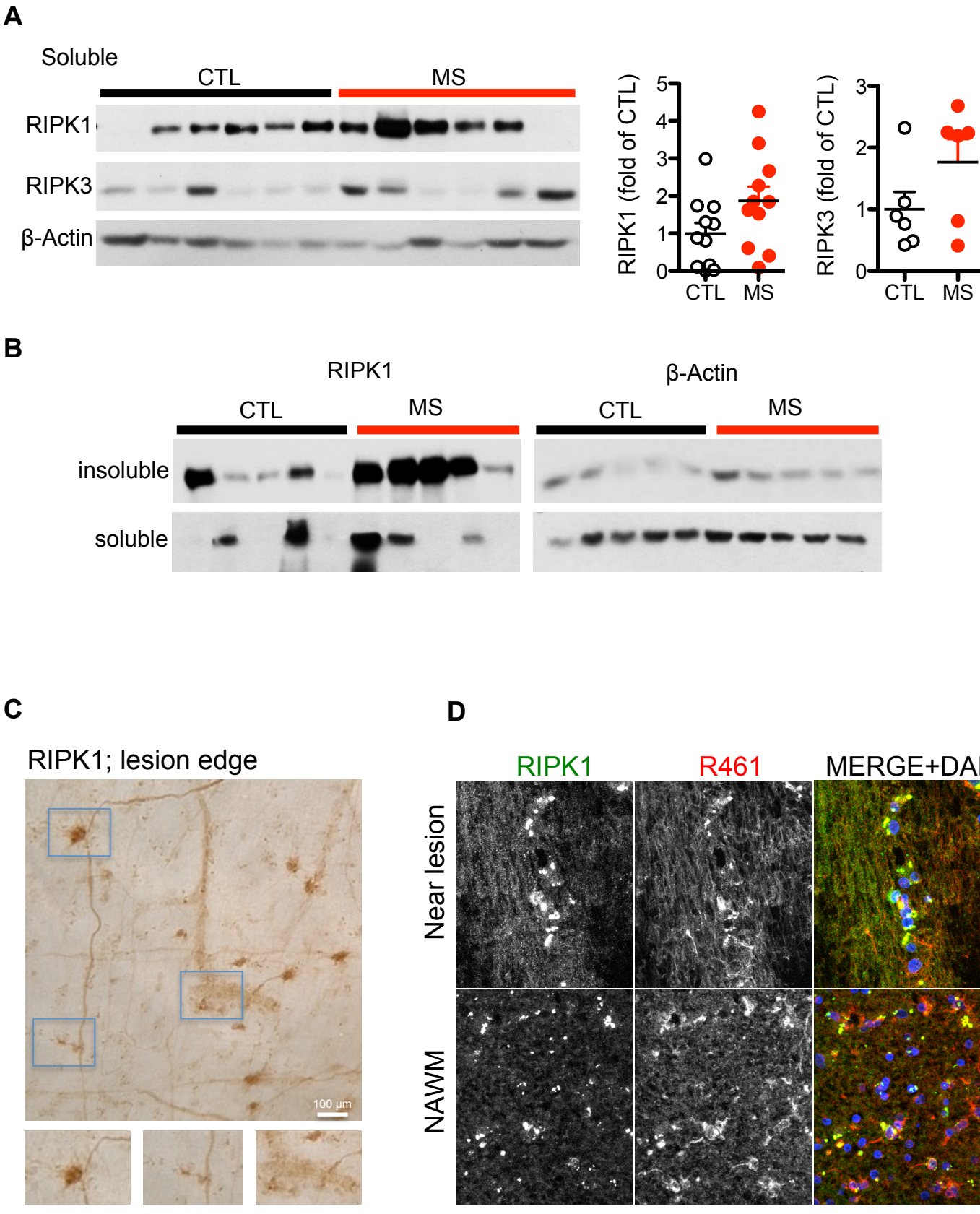
A
Soluble
CTL
MS
RIPK1
RIPK3
β-Actin
RIPK1 (fold of CTL)
RIPK3 (fold of CTL)
B
RIPK1
β-Actin
insoluble
soluble
C
RIPK1; lesion edge
100 µm
D
RIPK1
R461
MERGE+DAPI
Near lesion
NAWM

Figure S1

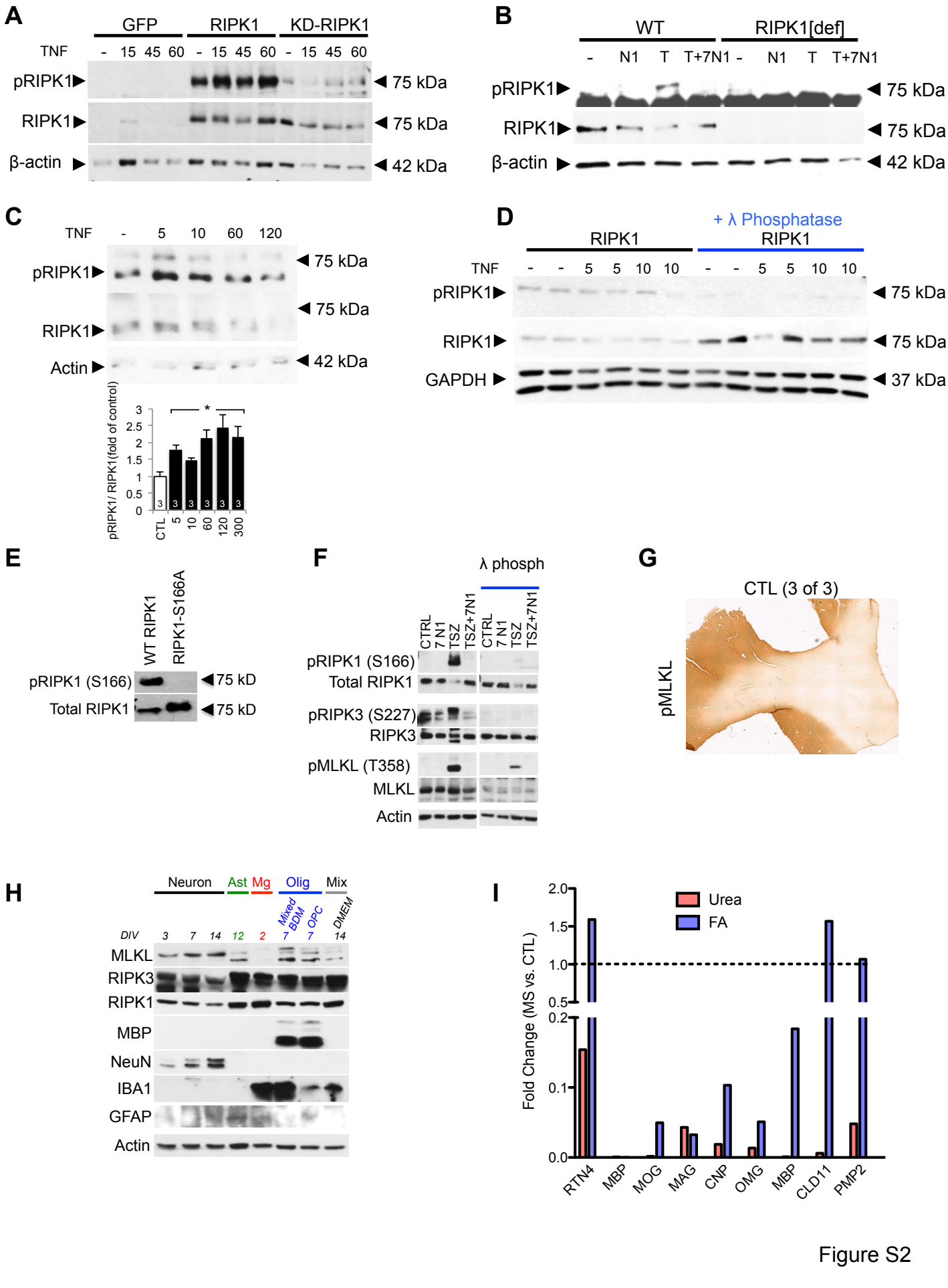
A
GFP
RIPK1
KD-RIPK1
TNF
- 15 45 60 - 15 45 60 - 15 45 60
pRIPK1
RIPK1
β-actin
75 kDa
75 kDa
42 kDa
B
WT
RIPK1[def]
- N1 T T+7N1 - N1 T T+7N1
pRIPK1
RIPK1
β-actin
75 kDa
75 kDa
42 kDa
C
TNF - 5 10 60 120
pRIPK1
RIPK1
Actin
75 kDa
75 kDa
42 kDa
pRIPK1/ RIPK1(fold of control)
CTL 5 10 60 120 300
D
RIPK1
+ λ Phosphatase
RIPK1
TNF
- - 5 5 10 10 - - 5 5 10 10
pRIPK1
RIPK1
GAPDH
75 kDa
75 kDa
37 kDa
E
WT RIPK1
RIPK1-S166A
pRIPK1 (S166)
Total RIPK1
75 kD
75 kD
F
λ phosph
CTRL 7 N1 TSZ TSZ+7N1 CTRL 7 N1 TSZ TSZ+7N1
pRIPK1 (S166)
Total RIPK1
pRIPK3 (S227)
RIPK3
pMLKL (T358)
MLKL
Actin
G
CTL (3 of 3)
pMLKL
H
Neuron
Ast
Mg
Olig
Mix
Mixed BDM
OPC
DMEM
DIV 3 7 14 12 2 7 7 14
MLKL
RIPK3
RIPK1
MBP
NeuN
IBA1
GFAP
Actin
I
Urea
FA
Fold Change (MS vs. CTL)
RTN4 MBP MOG MAG CNP OMG MBP CLD11 PMP2

Figure S2

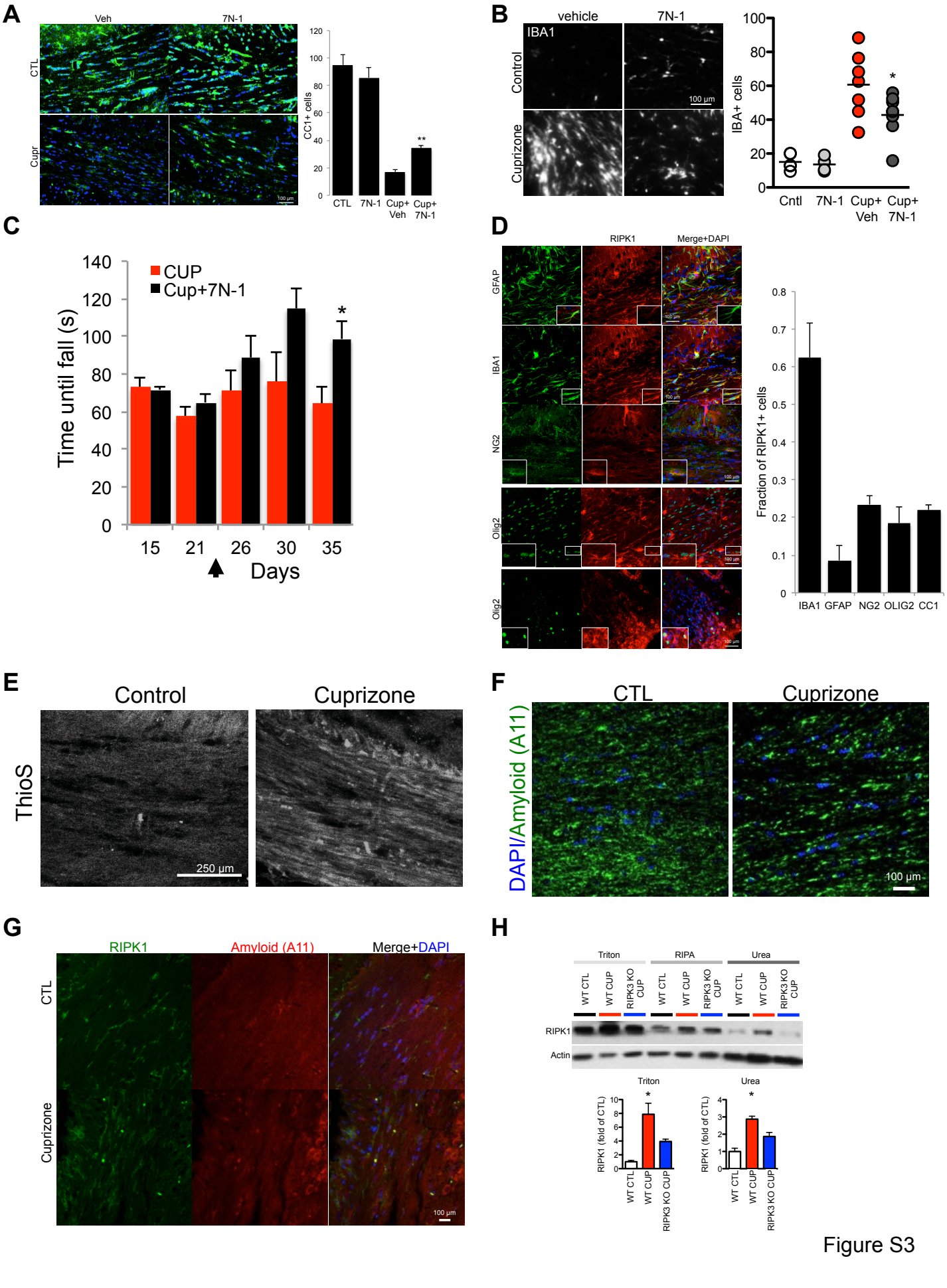
A
Veh
7N-1
CTL
Cupr
CC1+ cells
CTL
7N-1
Cup+ Veh
Cup+ 7N-1
B
vehicle
7N-1
IBA1
Control
Cuprizone
IBA1+ cells
Cntl
7N-1
Cup+ Veh
Cup+ 7N-1
C
CUP
Cup+7N-1
Time until fall (s)
Days
D
RIPK1
Merge+DAPI
GFAP
IBA1
NG2
Olig2
Olig2
Fraction of RIPK1+ cells
IBA1
GFAP
NG2
OLIG2
CC1
E
Control
Cuprizone
ThioS
250 µm
F
CTL
Cuprizone
DAPI/Amyloid (A11)
100 µm
G
RIPK1
Amyloid (A11)
Merge+DAPI
CTL
Cuprizone
100 µm
H
Triton
RIPA
Urea
WT CTL
WT CUP
RIPK3 KO CUP
RIPK1
Actin
Triton
Urea
RIPK1 (fold of CTL)
WT CTL
WT CUP
RIPK3 KO CUP

Figure S3

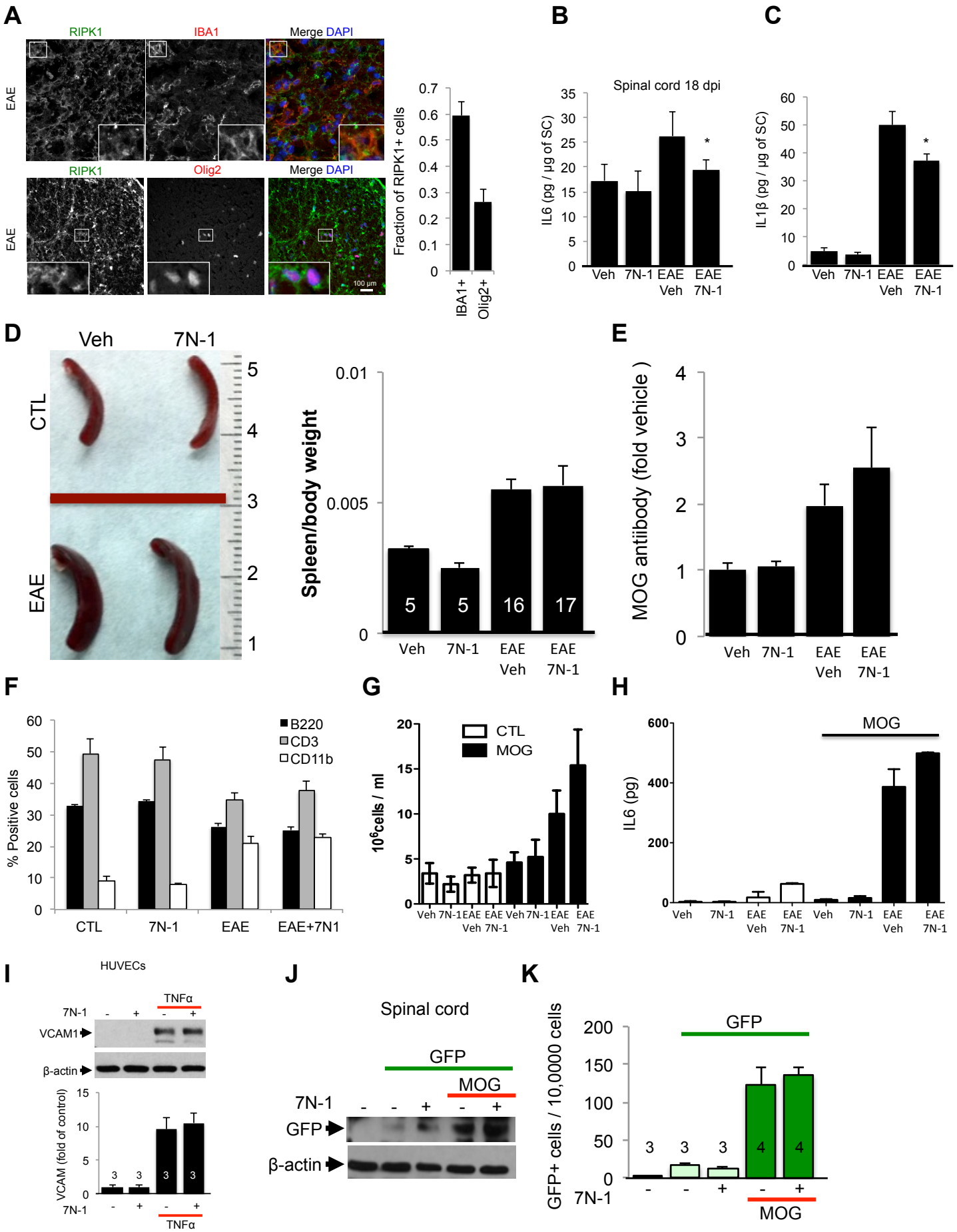
A
RIPK1
IBA1
Merge DAPI
EAE
RIPK1
Olig2
Merge DAPI
EAE
100 µm
Fraction of RIPK1+ cells
IBA1+
Olig2+
B
Spinal cord 18 dpi
IL6 (pg / µg of SC)
Veh
7N-1
EAE Veh
EAE 7N-1
C
IL1β (pg / µg of SC)
Veh
7N-1
EAE Veh
EAE 7N-1
D
Veh
7N-1
CTL
EAE
Spleen/body weight
5
5
16
17
Veh
7N-1
EAE Veh
EAE 7N-1
E
MOG antiibody (fold vehicle)
Veh
7N-1
EAE Veh
EAE 7N-1
F
% Positive cells
B220
CD3
CD11b
CTL
7N-1
EAE
EAE+7N1
G
CTL
MOG
10^6cells / ml
H
MOG
IL6 (pg)
I
HUVECs
TNFα
7N-1
VCAM1
β-actin
VCAM (fold of control)
TNFα
J
Spinal cord
GFP
MOG
7N-1
GFP
β-actin
K
GFP
GFP+ cells / 10,0000 cells
7N-1
MOG

Figure S4

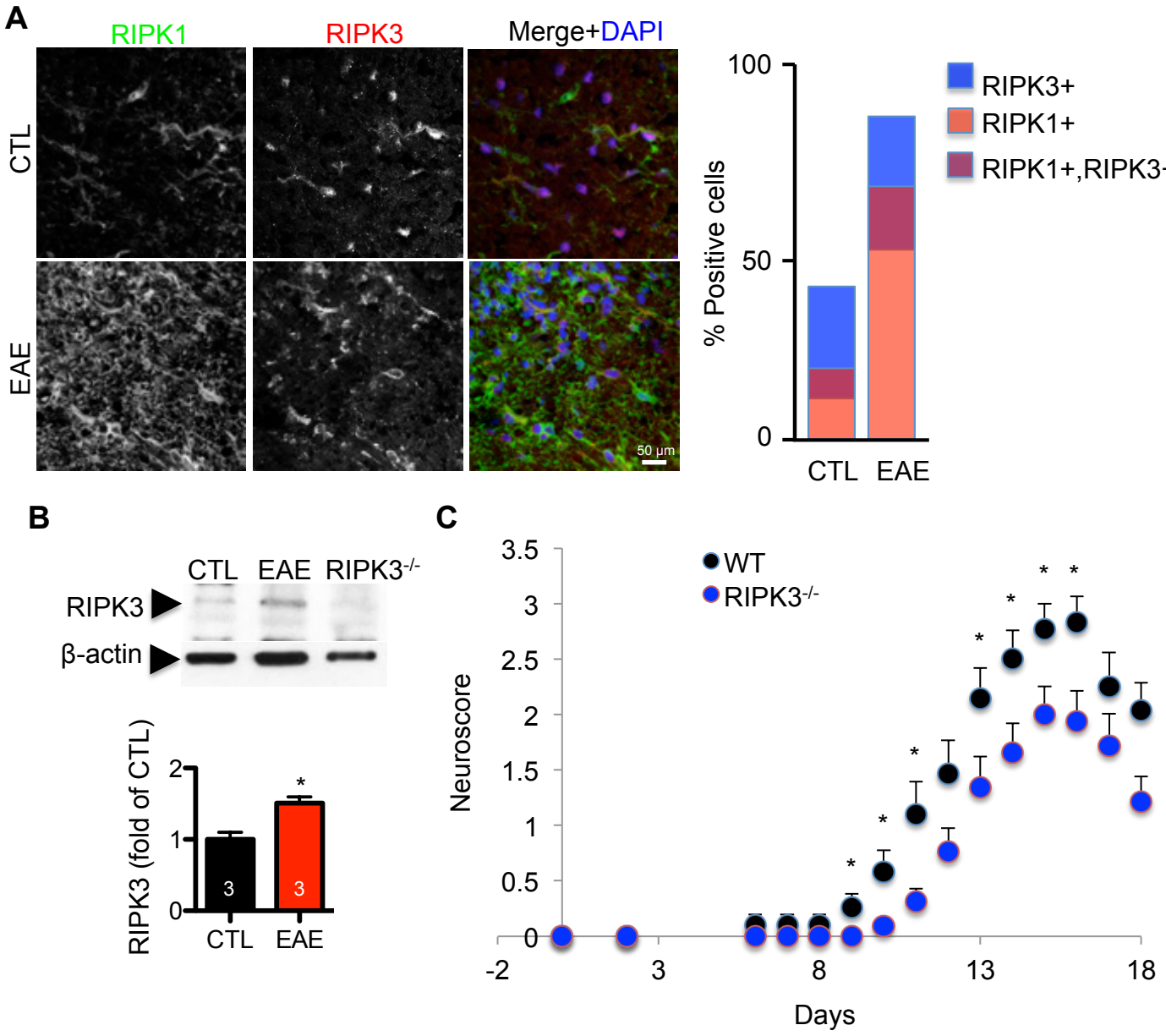

	B220	CD11b	CD3
WT	37.5	20	31.5
RIPK3 $^{-/-}$	32	18	31.5

Figure S5

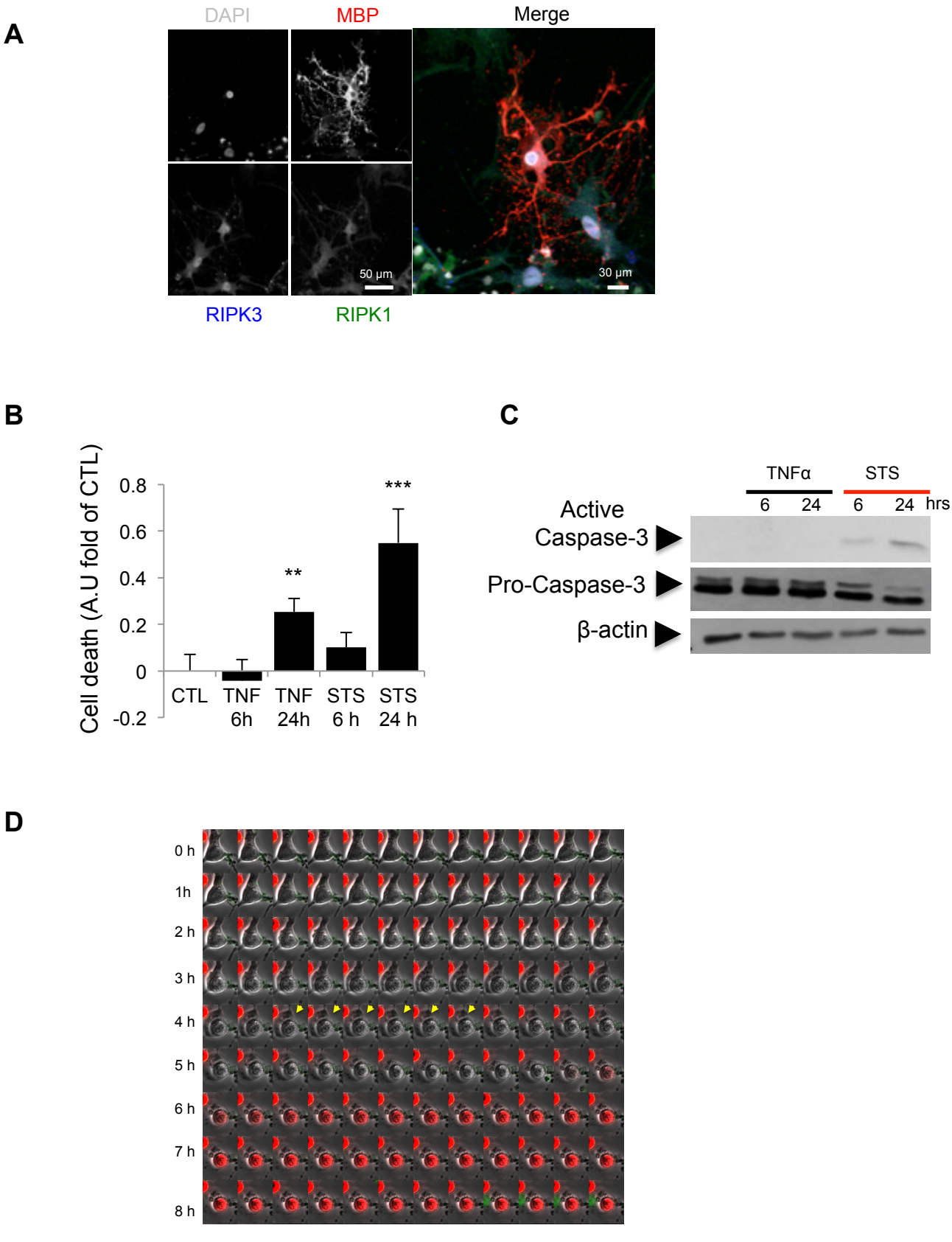
A
DAPI
MBP
Merge
50 µm
30 µm
RIPK3
RIPK1
B
Cell death (A.U fold of CTL)
0.8
0.6
0.4
0.2
0
-0.2
**
***
CTL
TNF 6h
TNF 24h
STS 6 h
STS 24 h
C
TNFα
STS
6
24
6
24
hrs
Active Caspase-3
Pro-Caspase-3
β-actin
D
0 h
1h
2 h
3 h
4 h
5 h
6 h
7 h
8 h

Figure S6

A

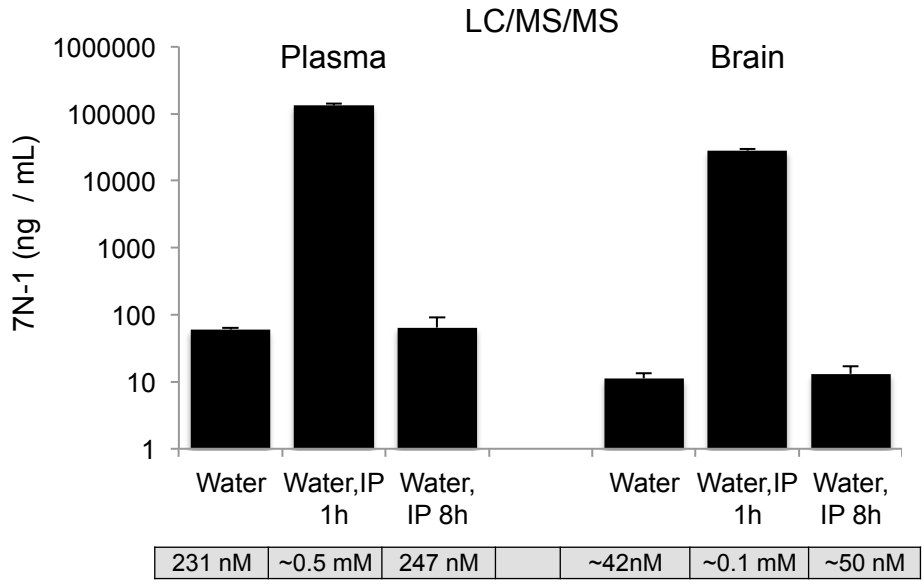

B

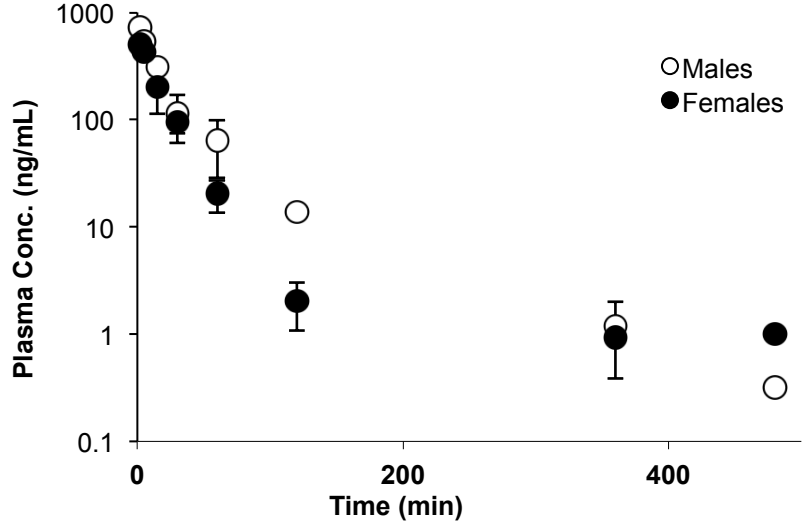

C

Pharmacokinetic Analysis

Table 3 -Pharmacokinetic Parameters for 7-Cl-O-Nec-1 – Males and Females

Group	Dose (mg/kg)	AUC_{8h} (min*ng/mL)	C_{max}** (ng/mL)	T_{max} (min)	$T_{1/2}$ (min)	V_{SS} ($mL.kg^{-1}$)	CLs ($mL.min^{-1}.kg^{-1}$)
Males	**1**	**16461.7**	**873.1**	**0**	**66.5**	**2494.8**	**60.6**
Females	**1**	**9921.4**	**573.1**	**0**	**ND**	**3345.5**	**100.0**

*AUC values normalized to dose

**Extrapolated Value (log linear)

Abbreviations: AUC 8 h – Area under the curve at 8 h; Cmax – estimated maximum plasma concentration; Tmax – time of maximum observed concentration; T ½ - terminal elimination half-life; Vss – Volume of distribution at steady state; Cls – systemic clearance.

Figure S7

Patient	RIPK1(s)	RIPK1(u)	RIPK3(u)	Casp-8	FLIP	Myelin
U-CTL-1	-	-	+	-	-	++++
U-CTL-2	+	+	+	+	-	++
U-CTL-3	+	+	+	-	-	++++
U-CTL-4	++	+	++	+	-	++
U-CTL-5	+	N/A	+	-	++	+++
U-CTL-6	++	N/A	+	-	+	++++
C-CTL-1	+	++	++	-	+	+
C-CTL-2	++	+	+	-	++	++++
C-CTL-3	-	+	+	-	-	++
C-CTL-4	+++	+	+	-	++	++
C-CTL-5	+	-	+	+	-	+++
U-MS-1	++	++++	++	-	+	++
U-MS-2	+++	+++	+++	+	++	-
U-MS-3	+++	++++	++	+++	+++	-
U-MS-4	++	+++	+	+++	+	-
U-MS-5	++	N/A	+++	++	++	+
U-MS-6	-	N/A	+	+++	+	++
C-MS-1	+++	++++	+++	+++	++	+
C-MS-2	+++	++++	+++	+++	+++	-
C-MS-3	+	+++	+++	-	+	+
C-MS-4	++	++++	++	++	++	++
C-MS-5	-	+	++	+++	+	++

Table S1

Upregulated genes in chronic active lesions vs. inactive lesions that are regulators of necroptosis

Gene Symbol	Entrez Gene ID	Accession #	Mean z-score
RNH1	107702	NM_145135	-6.387663682
ACE	11421	NM_009598	-3.63454219
TOP1	21969	NM_009408	-2.50715914
MST1	15235	NM_008243	-2.204035292
TNFSF10	22035	NM_009425	-2.201076593
GATA3	14462	NM_008091	-2.164057656
ZFP36	22695	NM_011756	-1.69244849
TCEA1	21399	NM_011541	-1.601099427
Ptk7	71461	NM_175168	-1.27703078
BRF1	72308	NM_028193	3.509477789
CASP9	12371	NM_015733	2.787101711
Sp1	20683	NM_013672	2.112424675
IL13	16163	NM_008355	2.065390789
HSF4	26386	NM_011939	1.741837716
HOXD3	15434	NM_010468	1.631447136
PRKAR1B	19085	NM_008923	1.471116448
EGR1	13653	NM_007913	1.466661463
CD4	12504	NM_013488	1.453573802
MAPK1	26413	NM_011949	1.431040168
FGFR1	14182	NM_010206	1.419384238

Proteins enriched by >1.5 fold (MS vs. CTL) in the urea fraction

AAK1	ATP2B1	CKB	DYNLT3	GLS	HSPH1	MT-CYB	PANK4	PSMC4	SLC1A3	TUBA1B	YWHAZ
AARS	ATP2B2	CKMT1B	ECHS1	GLUD1	IDH2	MT-ND2	PARP1	PSMC5	SLC25A1	TUBA1C	
AASDHPPT	ATP2B3	CLASP2	EEF1A1	GLUL	IDH3A	MT-ND4	PC	PSMC6	SLC25A11	TUBA3D	
ABAT	ATP2B4	CLTC	EEF1A2	GNA13	IDH3B	MT-ND5	PCBP2	PSMD11	SLC25A12	TUBA4A	
ABHD11	ATP5A1	CLU	EEF1D	GNAI1	IGHV4-31	MTCH1	PCYT2	PTPLAD1	SLC25A22	TUBA8	
ACAN	ATP5B	CMPK1	EEF1G	GNAI2	IMMT	MTCH2	PDCD6IP	PURA	SLC25A3	TUBAL3	
ACO2	ATP5C1	CNRIP1	EHD1	GNAI3	INA	MTHFD1	PDE1B	PYGB	SLC25A4	TUBB	
ACTB	ATP5D	CNTN1	EHD3	GNAO1	INPP1	MVP	PDHB	PYGM	SLC25A5	TUBB2A	
ACTC1	ATP5F1	CNTN2	EIF1	GNB1	IPO5	MYH10	PDIA3	RAB10	SLC25A6	TUBB2B	
ACTG1	ATP5H	COPS4	EIF1B	GNB2	IPO7	MYH9	PDK3	RAB14	SLC3A2	TUBB2C	
ACTR1A	ATP5L	CORO1A	EIF3F	GNB4	IPO9	MYO5A	PDXK	RAB3A	SLC4A4	TUBB3	
ACTR1B	ATP5O	COX4I1	EIF4A1	GNG12	IQSEC1	NAGK	PEA15	RAB7A	SNAP25	TUBB4	
ACTR2	ATP6V0A1	COX5A	EIF4H	GNL1	KCNAB2	NAMPT	PFKL	RAC1	SNAP91	TUBB6	
ACTR3	ATP6V1A	COX5B	EIF5A	GPI	KIAA1045	NAP1L1	PFKM	RAD23A	SNORA41	TUBB8	
ADD1	ATP6V1B2	COX6B1	ELAVL1	GPM6A	KIAA1468	NCDN	PFKP	RANBP1	SNTA1	TUBBP5	
ADD3	ATP6V1C1	COX7A1	ENO1	GSN	KIAA1598	NDRG2	PFN1	RANP1	SOD2	TUFM	
AHSA1	ATP6V1E1	CPLX2	ENO2	GSTM1	KIF21A	NDUFA10	PFN2	RAP1GDS1	SPTAN1	TWF2	
AK1	BRP44	CRYAB	ENOPH1	GSTM2	KIF5B	NDUFA12	PGAM1	RAP2A	SPTBN1	TXNDC5	
AK5	C10orf58	CSE1L	ENPP6	GSTM3	KIF5C	NDUFA13	PGK1	RAP2B	SPTBN4	TXNRD1	
AKAP12	C11orf2	CST3	EPB41L1	GSTM4	KPNB1	NDUFA4	PGRMC1	RAPGEF2	SRGAP3	UBA1	
ALDH1L1	C1QBP	CSTB	EPB41L2	GUK1	KRAS	NDUFA5	PHB	RDH11	ST13	UBA6	
ALDH2	CA2	CTNNA2	EPB41L3	H2AFX	KRT78	NDUFA9	PHB2	REEP2	ST13P4	UBE2N	
ALDH6A1	CALR	CTNNB1	EPS15	H2AFY	LAP3	NDUFB10	PHGDH	RHOA	STAM	UBXN6	
ALDOA	CAMK1D	CTNND1	ERLIN2	H3F3A	LGALS1	NDUFB11	PHYHIPL	RHOB	STK39	UCHL1	
ALDOC	CAMK2A	CTNND2	ESD	HADHA	LGI1	NDUFS1	PIK3R1	RHOC	STOM	UQCRB	
AMPH	CAMK2B	CYB5B	ESYT1	HEPACAM	LHPP	NDUFS2	PIN1	RHOG	STX1B	UQCRC1	
ANK2	CAMK2D	DCLK1	EZR	HIST2H2AB	LLGL1	NDUFS3	PKP4	RNH1	STXBP1	UQCRC2	
ANLN	CAMK2G	DCLK2	FAM49A	HIST2H4B	LONP1	NDUFS5	PLEC	RPL13	SUCLA2	UQCRFS1	
ANXA1	CAMKV	DCTN1	FASN	HK1	LRPPRC	NDUFV1	PLEKHB1	RPL27A	SUCLG1	UQCRH	
ANXA5	CANX	DCTN2	FBXO2	HNRNPA1	LY6H	NDUFV2	PMVK	RPL6	SUGT1	USMG5	
ANXA6	CAP1	DCXR	FHL1	HNRNPA2B1	MAOB	NEFH	PPIA	RPLP1	SYN1	USO1	
AP2A1	CAP2	DDX1	FKBP1A	HNRNPC	MAP1A	NEFL	PPP1CB	RPS13	SYN2	USP24	
AP2A2	CARNS1	DDX3X	FKBP4	HNRNPH1	MAP1B	NEFM	PPP1CC	RRAS	SYNJ1	USP5	
AP3M2	CARS	DIRAS2	FLOT1	HNRNPH2	MAP2	NEGR1	PPP1R7	RRAS2	TAGLN2	VAPB	
AQP1	CAV1	DLD	FSCN1	HNRNPH3	MAP2K1	NFASC	PPP2CA	RTN1	TAGLN3	VARS	
AQP4	CBR1	DNM1	FSD1L	HNRNPK	MAPK3	NIPSNAP1	PPP2R1A	RUFY3	TBCB	VCAN	
ARF3	CCT2	DNM1L	FXYD6	HNRNPL	MAPRE2	NNT	PPP2R2A	S100A8	THY1	VDAC1	
ARHGAP1	CCT3	DNM2	FXYD6-FXYD2	HNRNPU	MAPRE3	NRAS	PPP2R4	SAMM50	TKT	VDAC2	
ARHGDIA	CCT4	DNM3	FYN	HP	MARCKS	NRBP1	PPP2R5D	SBF1	TLN1	VDAC3	
ARL1	CCT6A	DOCK3	GAN	HPCAL4	MATR3	NRBP2	PPP2R5E	SCRN1	TLN2	VGF	
ARL8A	CD59	DPYSL2	GANAB	HRAS	MC1R	NSF	PRDX3	SDR39U1	TMOD2	VIM	
ARPC5L	CD81	DPYSL3	GAP43	HSP90AA1	MDH2	NTM	PRDX5	SESTD1	TNR	VPS52	
ASNA1	CD9	DPYSL4	GAPDH	HSP90AB1	METTL7A	NUMA1	PREPL	SFXN1	TOLLIP	VTA1	
ATIC	CDC42	DST	GDAP1	HSPA12A	MGST3	OGDH	PRKACB	SFXN3	TOM1	WDR1	
ATL1	CDS2	DSTN	GDAP1L1	HSPA1B	MIR1248	OLA1	PRKAG1	SH3BGRL3	TOM1L2	XPO1	
ATP1A1	CEP170	DYNC1H1	GFAP	HSPA1L	MLC1	OSTF1	PRKAR1A	SH3GL2	TPI1	YWHAB	
ATP1A2	CFL1	DYNC1I1	GIT1	HSPA8	MOBP	OTUB1	PRKCA	SH3GLB2	TPPP	YWHAE	
ATP1A3	CHMP5	DYNC1I2	GJA1	HSPA9	MSN	OXCT1	PRKCB	SIRT5	TPRG1L	YWHAG	
ATP1B1	CISD1	DYNC1LI2	GLIPR2	HSPB1	MT-CO2	PAFAH1B3	PRKCG	SLC14A1	TRIM2	YWHAH	
ATP2A2	CKAP5	DYNLL1	GLO1	HSPB6	MT-CO3	PALM	PSMA2	SLC1A2	TUBA1A	YWHAQ	

Table S3

Increased components in the insoluble proteome of MS that were also found in Lewy body of pathological brain samples from PD patients.

AARS	COPB1	GPI	PLEC	VPS35
ABCD3	COPB2	GSN	POR	WDR1
ACOT7	COPZ1	GSTM3	PPP2R4	WDR7
ACTN1	CORO1A	HIBCH	PRDX3	XPO1
ACTR2	CPT2	HNRNPD	PRDX5	YWHAE
ADD1	CRYM	HSD17B10	PRKCB	
ADD3	CSE1L	HSDL2	PRODH	
ADSS	CTNNA2	HSP90AB1	PROSC	
AFG3L2	CTNND1	HSPA4L	PSMC6	
AIDA	CTSD	HSPB1	PSMD2	
AKR1A1	DCLK1	IPO5	PYGB	
AKR1C1	DCTN1	IPO7	RAB23	
ALDH4A1	DCTN2	KARS	RAN	
ALDH6A1	DDX1	LASP1	RAP1GDS1	
ALDOC	DGKB	MACF1	RCN1	
ANKFY1	DNAJB1	MAP1A	ROCK2	
ANXA6	DNM1L	MAP1B	RTN1	
AP2A1	DPYSL2	MAP2K1	SAR1A	
AP2B1	DTNA	MFN2	SDHB	
AP3S1	DYNC1H1	MPP6	SEC22B	
ARHGDIA	DYNC1I1	MTCH2	SH3GL2	
ARMC10	DYNC1LI2	MTHFD1	SH3GLB2	
ATIC	EEF1A2	MYH10	SNTA1	
ATL1	EEF2	NANS	SPTAN1	
ATP2A2	EHD3	NAPB	SPTBN1	
ATP6V1A	ELMO1	NCDN	STUB1	
ATP6V1B2	ELMO2	NNT	SYN1	
ATP6V1E1	ENO1	NUDC	TBCB	
BLVRB	EPRS	OPA1	TCP1	
CA1	EXOC8	OTUB1	THNSL1	
CADPS	FAM49A	PAFAH1B1	TLN2	
CANX	FARSB	PDE1B	TPI1	
CAP1	FASN	PDIA3	TPP1	
CBR1	FBXO2	PDIA6	TPPP	
CCT2	FERMT3	PDK2	TRAP1	
CDH2	FH	PDXK	UBA1	
CFL1	FKBP2	PFN1	UCHL1	
CLIC4	FSCN1	PGAM1	USO1	
CLTC	FUK	PGRMC1	VAPB	
COPA	GANAB	PHGDH	VARS	

Proteins enriched by >1.5 fold (MS vs. CTL) in the urea fraction that are associated with PD, HD or AD

AP2A1	COX5A	NDUFB10	UBA1
AP2A2	COX5B	NDUFS1	UCHL1
ATP2A2	COX6B1	NDUFS2	UQCR
ATP5A1	COX7A1	NDUFS3	UQCRB
ATP5B	DCTN1	NDUFS5	UQCRC1
ATP5C1	DCTN2	NDUFV1	UQCRFS1
ATP5D	GAPDH	NDUFV2	UQCRH
ATP5F1	MAPK3	PIN1	VDAC1
ATP5H	NDUFA10	SLC25A4	VDAC2
ATP5O	NDUFA4	SLC25A5	VDAC3
CLTC	NDUFA5	SLC25A6	UQCRC2
COX4I1	NDUFA9	SOD2	

Table S5

Putative RIPK3 targets in MS urea fraction

	Site/motif
ADD1	S358
ANK2	S1461
AP3B2	S272
ARMC10	SY site
BASP1	T36
CLDN11	S198
CLNS1A	S102
CRYAB	SW site
CTNNA2	S640
DAAM2	S656
DNAJC5	S10
DYNC1I1	S179
EEF1D	S162
EPB41L1	S678
EPB41L2	S39
EPB41L3	S708
GIT1	S362
HEPACAM	SL site

	Site/motif
HNRNPC	SA site
HSP90AA1	S263
HSP90AB1	S226
MAP1A	S909
MAP1B	S832
MAP2	S136
MLF2	S238
NEFH	S503
OSTF1	S213
PLCL1	T556
PRKCA	SF site
PTGES3	S113
RPLP1	S101
RPLP2	S102
SEPTIN2	S218
STX1A	S14
STX1B	S14
UFL1	S458